



OMI-measured increasing SO₂ emissions due to energy industry expansion and relocation in northwestern China

Zaili Ling¹, Tao Huang¹, Yuan Zhao¹, Jixiang Li¹, Xiaodong Zhang¹, Jinxiang Wang¹, Lulu Lian¹, Xiaoxuan Mao¹, Hong Gao¹, and Jianmin Ma^{2,1,3}

¹Key Laboratory for Environmental Pollution Prediction and Control, Gansu Province, College of Earth and Environmental Sciences, Lanzhou University, 730000 Lanzhou, China

²Laboratory for Earth Surface Processes, College of Urban and Environmental Sciences, Peking University, 100871 Beijing, China

³CAS Center for Excellence in Tibetan Plateau Earth Sciences, Chinese Academy of Sciences, 100101 Beijing, China

Correspondence to: Jianmin Ma (jianminma@lzu.edu.cn) and Tao Huang (huanagt@lzu.edu.cn)

Received: 19 February 2017 – Discussion started: 29 March 2017

Revised: 25 June 2017 – Accepted: 3 July 2017 – Published: 27 July 2017

Abstract. The rapid growth of economy makes China the largest energy consumer and sulfur dioxide (SO₂) emitter in the world. In this study, we estimated the trends and step changes in the planetary boundary layer (PBL) vertical column density (VCD) of SO₂ from 2005 to 2015 over China measured by the Ozone Monitoring Instrument (OMI). We show that these trends and step change years coincide with the effective date and period of the national strategy for energy development and relocation in northwestern China and the regulations in the reduction of SO₂ emissions. Under the national regulations for the reduction of SO₂ emissions in eastern and southern China, SO₂ VCD in the Pearl River Delta (PRD) of southern China exhibited the largest decline during 2005–2015 at a rate of $-7\% \text{ yr}^{-1}$, followed by the North China Plain (NCP) ($-6.7\% \text{ yr}^{-1}$), Sichuan Basin ($-6.3\% \text{ yr}^{-1}$), and Yangtze River Delta (YRD) ($-6\% \text{ yr}^{-1}$). The Mann–Kendall (MK) test reveals the step change points of declining SO₂ VCD in 2009 for the PRD and 2012–2013 for eastern China responding to the implementation of SO₂ control regulation in these regions. In contrast, the MK test and regression analysis also revealed increasing trends of SO₂ VCD in northwestern China, particularly for several “hot spots” featured by growing SO₂ VCD in those large-scale energy industry bases in northwestern China. The enhanced SO₂ VCD is potentially attributable to increasing SO₂ emissions due to the development of large-scale energy industry bases in energy-abundant northwestern China under the national strategy for the energy

safety of China in the 21st century. We show that these large-scale energy industry bases could overwhelm the trends and changes in provincial total SO₂ emissions in northwestern China and contribute increasingly to the national total SO₂ emissions in China. Given that northwestern China is more ecologically fragile and uniquely susceptible to atmospheric pollution than the rest of China, increasing SO₂ emissions in this part of China should not be overlooked and merit scientific research.

1 Introduction

Sulfur dioxide (SO₂) is one of the criteria air pollutants emitted from both anthropogenic and natural sources. The combustion of sulfur-containing fuels, such as coal and oil, is the primary anthropogenic emitter, which contributes to half of total SO₂ emissions (Smith et al., 2011; Lu et al., 2010; Stevenson et al., 2003; Whelpdale et al., 1996). With the rapid economic growth in the past decades, China has become the world's largest energy consumer, accounting for 23 % of global energy consumption in 2015 (BIEE, 2016). Coal has been a dominating energy source in China and accounted for 70 % of total energy consumption in 2010 (Kanada et al., 2013). The huge demand for coal and its high sulfur content make China the largest SO₂ emission source in the world (Krotkov et al., 2016; Su et al., 2011), also accounting for two thirds of Asia's total SO₂ emissions (Ohara et al.,

2007). From 2000 to 2006, the total SO₂ emissions in China increased by 53 % at an annual growth rate of 7.3 % (Lu et al., 2010). To reduce SO₂ emissions, from 2005 onward the Chinese government has issued and implemented a series of regulations, strategies, and SO₂ control measures, leading to a drastic decrease of SO₂ emissions, particularly in eastern and southern China (Lu et al., 2011; Li et al., 2010).

Recently, two research groups led by NASA (National Aeronautics and Space Administration) and Lanzhou University of China published almost simultaneously the temporal and spatial trends of SO₂ in China from 2005 to 2015 using the OMI-retrieved SO₂ planetary boundary layer (PBL) column density after the OMI has been in use for 11 years (Krotkov et al., 2016; Shen et al., 2016). The results reported by the two groups revealed the widespread decline of SO₂ in eastern China for the past decade. Shen et al. noticed, however, that, in contrast to dramatic decreasing SO₂ emissions in densely populated and industrialized eastern and southern China, the OMI-measured SO₂ in northwestern China appeared not to show a decreasing trend. This likely resulted from energy industry relocation and development in energy-abundant northwestern China in the past decades under the national strategy for China's energy development and safety during the 21st century. Concern has been raised about the potential impact of SO₂ emissions on the ecological environment and health risk in northwestern China because high SO₂ emissions could otherwise damage the rigorous ecological environment in this part of China, featured by very low precipitation and sparse vegetation coverage which reduce considerably the atmospheric removal of air pollutants (Ma and Xu, 2017).

To assess and evaluate the risks to the ecological environment and public of the growing SO₂ emissions in northwestern China, it is necessary to investigate the spatiotemporal distributions of SO₂ concentrations and emissions. However, the ground measurements of ambient SO₂ are scarce temporally and spatially in China and often subject to significant errors and uncertainties. Due to the rapid progress in the remote sensing techniques, satellite retrieval of air pollutants has become a powerful tool for the assessment of emissions and spatiotemporal distributions of air pollutants. In recent several years, SO₂ column concentrations retrieved by the Ozone Monitoring Instrument (OMI, Airbus Defence and Space Netherlands B.V., Leiden, the Netherlands, embedded on Aura satellite) have been increasingly applied to elucidate the spatiotemporal variation of global and regional SO₂ levels and its emissions from large point sources and evaluate the effectiveness of SO₂ control policies and measures (Krotkov et al., 2016; McLinden et al., 2015, 2016; Ialongo et al., 2015; Fioletov et al., 2015, 2016; Wang et al., 2015; Li et al., 2010). The decadal operation of the OMI provides the relatively long-term SO₂ time series data with a high spatial resolution which are particularly useful for assessing the changes and trends in SO₂ emissions induced by national regulations and strategies. The present study aims

to (1) determine the spatiotemporal variations of SO₂ and its trend under the national plan for energy industry development in northwestern China by making use of the OMI-measured SO₂ data during 2005–2015 and (2) identify leading causes contributing to the enhanced SO₂ emissions in northwestern China.

2 Data and methods

2.1 Satellite data

The OMI was launched on 15 July 2004 on the EOS Aura satellite, which is in a sun-synchronous ascending polar orbit with 13:45 local Equator crossing time. It is an ultraviolet–visible (UV–vis) nadir solar backscatter spectrometer, which provides nearly global coverage in 1 day, with a spatial resolution of 13 km × 24 km (Levelt et al. 2006a, b). It provides global measurements of ozone (O₃), SO₂, NO₂, HCHO, and other pollutants on a daily basis. The OMI uses spectral measurements between 310.5 and 340 nm in the UV-2 to detect anthropogenic SO₂ pollution in the lowest part of the atmosphere (Li et al., 2013). The instrument is sensitive enough to detect the near-surface SO₂. Previously, the OMI PBL SO₂ data were produced using the band residual difference (BRD) algorithm (Krotkov et al., 2006), which has large noise and unphysical biases particularly at high latitudes (Krotkov et al., 2008). Subsequently, a principal component analysis (PCA) algorithm was applied to retrieve SO₂ column densities. This approach greatly reduces biases and decreases the noise by a factor of 2, providing greater sensitivity to anthropogenic emissions (Li et al., 2013).

In the present study, we collected the level 3 OMI daily PBL SO₂ vertical column density (VCD) data in Dobson units (1 DU = 2.69 × 10¹⁶ molecules cm⁻²) produced by the PCA algorithm (Li et al., 2013). The spatial resolution is 0.25° × 0.25° latitude–longitude, available at Goddard Earth Sciences Data and Information Services Center (https://mirador.gsfc.nasa.gov/cgi-bin/mirador/presentNavigation.pl?tree=project&&dataGroup=L3_V003). The systematic bias of PCA retrievals is estimated as ~0.5 DU for regions between 30° S and 30° N. The bias increases to ~0.7–0.9 DU for high-latitude areas with large slant column O₃ but is still a factor of 2 smaller than that from BRD retrievals (https://aura.gesdisc.eosdis.nasa.gov/data/Aura_OMI_Level2/OMS02.003/doc/README.OMS02.pdf). As a result, the PCA algorithm may yield systematic errors for anthropogenic emission sources located in different latitudes and under complex topographic and underlying surface conditions. The air mass factors (AMFs) used to convert SO₂ slant column density into VCD are also subject to uncertainties. Fioletov et al. (2016) revealed an overall AMF uncertainty of 28 % which was created by surface reflectivity, surface pressure, ozone column, and cloud fraction. As Fioletov et al. (2016) noted, the PCA-retrieved

SO₂ VCD was virtually derived by using an AMF of 0.36, which is best applicable in the summertime in the eastern United States. Wang (2014) suggested adopting AMF ≈ 0.57 in the estimate of SO₂ VCD distribution in eastern China. In the present study, we have taken the AMF values in China provided by Fioletov et al. (2016) to adjust OMI-measured VCD in the estimation of the SO₂ emissions of the main point sources in northwestern China.

2.2 SO₂ monitoring, emissions, and socioeconomic data

To evaluate and verify the spatial SO₂ VCD from OMI, ground SO₂ monitoring data of 2014 through 2015 at 188 sampling sites (cities) across China (Fig. 1), operated by the National Environmental Monitoring Center were collected (available at <http://www.aqistudy.cn/historydata>). Annually averaged SO₂ air concentrations from 2005 to 2015 in six capital cities in Ürümqi (Xinjiang), Yinchuan (Ningxia), Beijing (Beijing–Tianjin–Hebei, BTH, and North China Plain, NCP), Shanghai (Yangtze River Delta, YRD), Guangzhou (Pearl River Delta, PRD), and Chongqing (Sichuan Basin) were collected from provincial environmental bulletin published by the Ministry of Environmental Protection of China (MEPC) (<http://www.zhb.gov.cn/hjzl/zghjzkgb/gshjzkgb>). SO₂ anthropogenic emission inventory in China with a 0.25° longitude by 0.25° latitude resolution for every 2 years from 2008 to 2012 was adopted from Multi-resolution Emission Inventory for China (MEIC) (Li et al., 2017, available at <http://www.meicmodel.org>).

The socioeconomic data in China were collected from the China Statistical Yearbooks and China Energy Statistical Yearbook, published by the National Bureau of Statistics of China (NBSC) (<http://www.stats.gov.cn/tjsj/ndsj/>; <http://tongji.cnki.net/kns55/Nav/HomePage.aspx?id=N2010080088&name=YCXME&floor=1>), as well as China National Environmental Protection Plan in the 11th 5-year plan (2006–2010) and 12th 5-year plan (2011–2015) released by MEPC (<http://www.zhb.gov.cn>). These data include industrial gross domestic product (GDP), coal consumption, thermal power generation, steel production, and SO₂ emission reduction plan, and they are presented in Table 1.

2.3 Trends and step change

The long-term trends of SO₂ VCD were estimated by linear regressions of the gridded annually SO₂ VCD against their time sequence of 2005 through 2015. The gridded slopes (trends) of the linear regressions denote the increasing (positive) or decreasing (negative) rates of SO₂ VCD (Wang et al., 2016; Huang et al., 2016; Zhang et al., 2015, 2016).

The Mann–Kendall (MK) test was also employed in the assessments of the temporal trend and step change point year of SO₂ VCD time series. The MK test is a nonparametric statistical test (Mann, 1945; Kendall and Charles, 1975) that is useful for assessing the significance of trends in time series

data (Waked et al., 2016; Fathian et al., 2016). The MK test is often used to detect a step change point in the long-term trend of a time series dataset (Moraes et al., 1998; Li et al., 2016; Zhao et al., 2015). It is suitable for non-normally distributed data and censored data which are not influenced by abnormal values (Yue and Pilon, 2004; Sharma et al., 2016; Yue and Wang, 2004; Gao and Shi, 2016; Zhao et al., 2015). Recently, the MK test has also been used in trend analysis for the time series of atmospheric chemicals, such as persistent organic pollutants, surface ozone (O₃), and non-methane hydrocarbon (Zhao et al., 2015; Assareh et al., 2016; Waked et al., 2016; Sicard et al., 2016). Here the MK test was used to identify the temporal variability and step change point of SO₂ VCD for 2005–2015 which may be associated with the implementation of the national strategy and regulation in energy industry development and emission control during this period. Under the null hypothesis (no trend), the test statistic was determined using the following formula:

$$S_k = \sum_{i=1}^k r_i (k = 2, 3, \dots, n), \quad (1)$$

where S_k is a statistic of the MK test, and

$$r_i = \begin{cases} +1, & (x_i > x_j) \\ 0, & (x_i \leq x_j) \end{cases} \quad (j = 1, 2, \dots, i - 1), \quad (2)$$

where x_i is the variable in time series $x_1, x_2, \dots, x_i, r_i$ is the cumulative number for $x_i > x_j$. The test statistic is normally distributed with a mean and variance is given by

$$E(S_k) = k(k - 1)/4, \quad (3)$$

$$\text{Var}(S_k) = \frac{k(k - 1)(2k + 5)}{72}. \quad (4)$$

From these two equations, one can derive a normalized S_i , defined by

$$\text{UF}_k = \frac{S_k - E(S_k)}{\sqrt{\text{Var}(S_k)}} (k = 1, 2, \dots, n), \quad (5)$$

where UF_k is the forward sequence, the backward sequence UB_k is calculated using the same function but with the reverse data series such that $\text{UB}_k = -\text{UF}_k$.

In a two-sided trend test, a null hypothesis is accepted at the significance level if $|\text{UF}_k| \leq (\text{UF}_k)_{1-\alpha/2}$, where $(\text{UF}_k)_{1-\alpha/2}$ is the critical value of the standard normal distribution, with a probability of α . When the null hypothesis is rejected (i.e., when any of the points in UF_k exceeds the confidence interval ± 1.96 ; $P = 0.05$), a significantly increasing or decreasing trend is determined. $\text{UF}_k > 0$ often indicates an increasing trend and vice versa. The test statistic used in the present study enables us to discriminate the approximate time of trend and step change by locating the intersection of the UF_k and UB_k curves. The intersection occurring within the confidence interval $(-1.96, 1.96)$ indicates the beginning of a step change point (Moraes et al., 1998; Zhang et al., 2011; Zhao et al., 2015).

Table 1. Annual growth rate for OMI SO₂ VCD and economic activities for individual provinces and municipality during 2005–2014 (% yr⁻¹), and SO₂ emission reduction plan during the 11th and 12th 5-year-plan periods (%).

Region		OMI SO ₂	Coal	Industrial	Thermal	Steel	SO ₂ emission reduction	
		VCD	consumption	GDP	power	production	plan (%)	
					generation		2006–2010 ^a	2011–2015 ^b
Northwestern	Inner Mongolia	0.94	11.29	20.48	14.07	8.38	-3.8	-3.8
	Shaanxi	-3.41	13.14	19.96	13.01	14.48	-12	-7.9
	Gansu	-0.09	6.69	14.19	8.89	9.92	0	2.0
	Qinghai	0.69	11.20	18.70	9.88	12.37	0	16.7
	Ningxia	0.95	11.79	17.44	15.04	152.71	-9.3	-3.6
	Xinjiang	1.57	17.21	14.21	23.39	16.27	0	0
BTH	Beijing	-3.59	-6.13	9.13	5.99	-48.52	-20.4	-13.4
	Tianjin	-4.63	3.15	15.84	6.01	10.19	-9.4	-9.4
	Hebei	-5.05	4.16	12.37	6.22	10.70	-15	-12.7
YRD	Shanghai	-7.65	-0.93	6.64	0.86	-0.92	-26.9	-13.7
	Jiangsu	-5.93	5.39	12.51	7.49	13.35	-18.0	-14.8
	Zhejiang	-2.07	4.04	11.40	8.68	13.94	-15.0	-13.3
PRD	Guangdong	-4.55	6.15	12.03	5.92	6.87	-15.0	-14.8

^a and ^b represent proposed reduction in SO₂ emissions in 2010 relative to 2005 and 2015 relative to 2010, respectively. The value for PRD refers to the proposed target for Guangdong province.

2.4 Estimate of SO₂ emissions from OMI measurements

To assess the connections between the major point sources in large-scale energy industrial bases in northwestern China and provincial emissions, we made use of OMI-measured SO₂ VCD to inversely simulate the SO₂ emissions from Ningdong Energy Chemical Industrial Base (NECIB) in Ningxia and Midong Energy Industrial Base (MEIB) in Xinjiang. McLinden et al. (2016) and Fioletov et al. (2015, 2016) have developed a source detection algorithm which fits OMI-measured SO₂ vertical column densities to a three-dimensional parameterization function of the horizontal coordinates and wind speed. This algorithm was employed in the present study to estimate the SO₂ source strength in the two industrial bases and its contribution to the provincial total SO₂ emissions. The details of this algorithm are in Fioletov et al. (2015). Briefly, the source detection algorithm uses a Gaussian function $f(x, y)$ multiplied by an exponentially modified Gaussian function $g(y, s)$ to fit the OMI SO₂ measurements (Fioletov et al., 2015) $OMI_{SO_2} = a \cdot f(x, y) \cdot g(y, s)$, defined by

$$\begin{aligned}
 f(x, y) &= \frac{1}{\sigma_1 \sqrt{2\pi}} \exp\left(-\frac{x^2}{2\sigma_1^2}\right); \\
 g(y, s) &= \frac{\lambda_1}{2} \exp\left(\frac{\lambda_1(\lambda_1 \sigma^2 + 2y)}{2}\right) \cdot \operatorname{erfc}\left(\frac{\lambda_1 \sigma^2 + y}{\sqrt{2}\sigma}\right); \\
 \sigma_1 &= \begin{cases} \sqrt{\sigma^2 - 1.5y}, & y < 0; \\ \sigma, & y \geq 0; \end{cases} \\
 \lambda_1 &= \lambda/s; \\
 \operatorname{erfc}(x) &= \frac{2}{\sqrt{\pi}} \int_x^\infty e^{-t^2} dt,
 \end{aligned} \tag{6}$$

where x and y indicate the coordinates of the OMI pixel center (km); s is the wind speed (km h⁻¹) at the pixel center; a represents the total number of SO₂ molecules (or SO₂ burden) observed by OMI in a target emission source $\lambda = 1/\tau$, where τ is a decay time of SO₂; and σ describes the width or spread of SO₂.

The $f(x, y)$ function represents the Gaussian distribution across the wind direction line. The function $g(y, s)$ represents an exponential decay along the y axis smoothed by a Gaussian function. Once σ and τ are determined, the SO₂ burden as a function of x , y , and s (OMI SO₂ (x, y, s)) can be reconstructed. SO₂ emission strength from a large point source can be estimated by $E = a/\tau$. In the present study, following Fioletov et al. (2016), we choose a mean value of $\sigma = 20$ km and $\tau = 6$ h in the calculation of SO₂ emission large point sources of interested. Wind speed and direction on a 1° × 1° latitude–longitude spatial resolution were collected from NCEP (National Centers for Environmental Prediction) Final Operational Global Analysis (<https://rda.ucar.edu/datasets/ds083.2/>). These data were interpolated to the location of each OMI pixel center on a 1/4° × 1/4° latitude–longitude spacing.

There are several potential sources of errors which need to be taken into account when determining the overall uncertainty of the SO₂ emission estimation. Fioletov et al. (2016) have highlighted three primary sources of errors in the OMI-based emission estimates, including AMF, the estimation of the total SO₂ mass as determined from a linear regression, and the selection of σ and τ used to fit OMI measurements. Based on the coefficients of variation (CV, %) in these three error categories (McLinden et al., 2014, 2016; Fioletov et

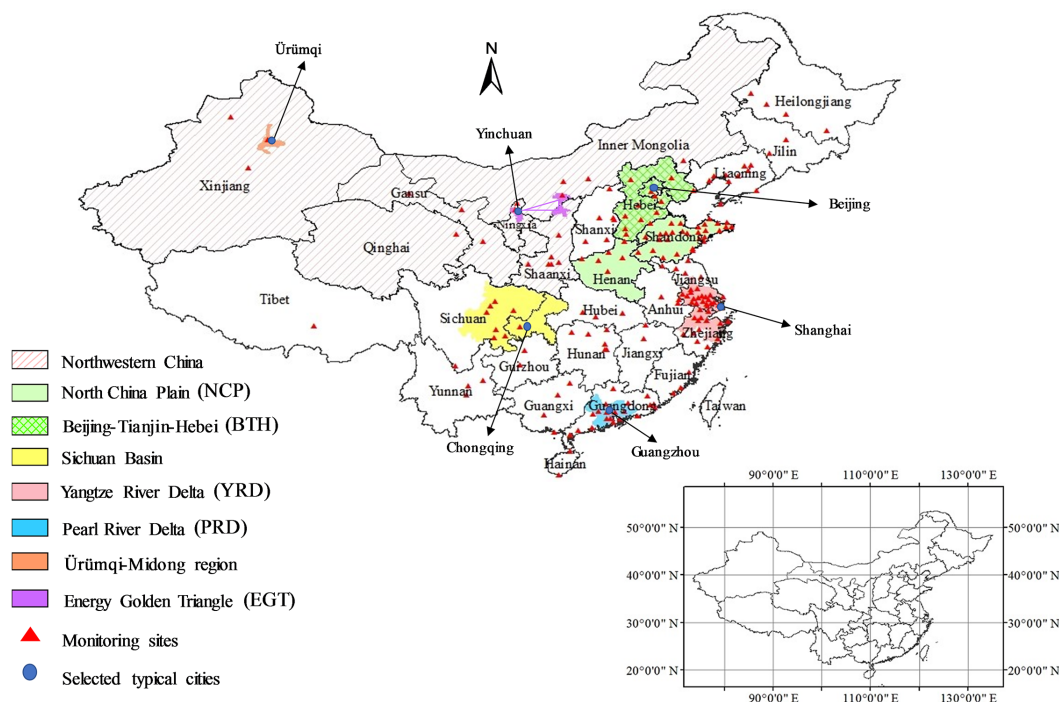


Figure 1. Selected regions in this investigation across China, including northwestern China, defined by slash, which includes Inner Mongolia, Shaanxi, Gansu, Qinghai, Ningxia, Beijing–Tianjin–Hebei (BTH), the North China Plain (NCP), the Sichuan Basin, Yangtze River Delta (YRD), and Pearl River Delta (PRD). These regions are labeled in the figure and marked by different colors. The Ürümqi–Midong region (brown) and the Energy Golden Triangle (EGT, purple) are also labeled in the figure. Red triangles indicate 188 monitoring sites across China. Blue circles indicate six selected cities in Fig. 2.

al., 2016) listed in Table S1 of Supplement, we estimated uncertainties in the SO₂ emissions derived from OMI measurements in the two major point sources in northwestern China by running the source detection model repeatedly for 10 000 times using the Monte Carlo method. Results show the standard deviation of -35 to 122 kt yr⁻¹ for SO₂ emissions in NECIB and -29 to 95 kt yr⁻¹ for SO₂ emissions in MEIB from 2005 to 2015, respectively.

2.5 Satellite data validation

The OMI-retrieved SO₂ PBL VCDs were evaluated by comparing with ambient air concentration data of SO₂ from routine measurements by local official operational air quality monitoring stations. The statistics between OMI-retrieved SO₂ VCD and monitored annually averaged SO₂ air concentrations during 2014–2015 at 188 operational air quality monitoring stations across China are presented in Table S2. Supplement Fig. S1 is the correlation diagram between SO₂ VCD and sampled data. As shown in Table S2 and Fig. S1, the OMI-measured SO₂ VCDs agree well with the monitored ambient SO₂ concentrations across China at the correlation coefficient of 0.85 ($p < 0.05$) (Table S2). Figure 2 further compares annually averaged SO₂ VCD and SO₂ air concentrations from 2005 to 2015 in six capital cities. These

are Ürümqi, Yinchuan, Beijing, Shanghai, Guangzhou, and Chongqing. The mean SO₂ concentration data were collected from provincial environmental bulletin published by the MEPC (<http://www.zhb.gov.cn/hjzl/zghjzkqb/gshjzkqb>). Results show that the annual variation of mean SO₂ VCD are higher than the measured SO₂ concentrations from 2010 to 2015, but SO₂ VCD match well with the monitored data except for Ürümqi, the capital of Xinjiang Uyghur Autonomous Region. The OMI-retrieved SO₂ VCDs in Shanghai and Chongqing are higher than the measured concentrations in these two regions show consistent temporal fluctuation and trend. The measured SO₂ concentrations peaked in 2013 in Yinchuan whereas the SO₂ VCD reached the peak in 2012 and decreased thereafter. OMI-measured SO₂ VCD in Ürümqi shows different yearly fluctuations compared with its annual concentrations. The measured SO₂ concentrations in Ürümqi decreased from 2011 to 2015 whereas the OMI-measured SO₂ VCD did not illustrate obvious changes. In particular, the monitored mean SO₂ concentration from 2013 to 2015 decreased by 75 % compared with that from 2005 to 2012. This is partly attributed to the change in air quality monitoring sites in the city of Ürümqi. Before 2013, there were only three operational air quality sites in Ürümqi, all located in the heavily polluted downtown region. Since 2013, the number of air monitoring sites

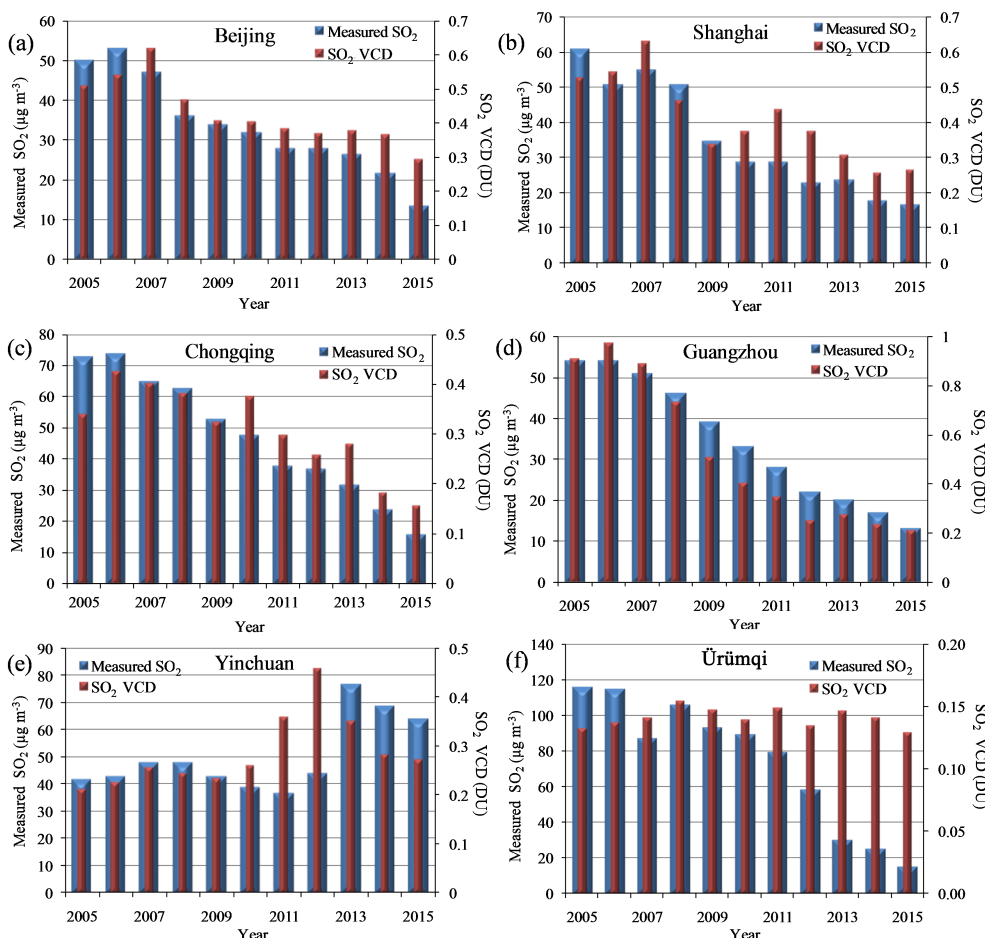


Figure 2. Annually averaged SO₂ VCD (DU), scaled on the right-hand-side y axis, and measured annual SO₂ air concentration ($\mu\text{g m}^{-3}$), scaled on the left-hand-side y axis, in Beijing, Shanghai, Chongqing, Guangzhou, Yinchuan, and Ürümqi.

increased from three to seven. The four new sites are located in less polluted suburbs of the city. As a result, the spatially averaged SO₂ concentrations over three downtown air quality monitoring sites before 2013 were higher than the mean concentrations averaged over seven monitoring sites (http://xjny.ts.cn/content/2012-06/05/content_6899388.htm).

It is worth noting that the measured SO₂ concentration in Ürümqi is the highest among all cities, as shown in Fig. 2, whereas the OMI VCD value in Ürümqi was lower than other selected cities. This may be due to systematic biases in OMI-retrieved SO₂ VCD. In the present study, the level 3 OMI PBL SO₂ VCD data produced by the PCA retrievals were used to estimate the spatiotemporal variation in SO₂ pollution in China. The PCA retrievals have a negative bias over some highly reflective surfaces in arid and semi-arid lands, such as many some places in the Sahara (up to about -0.5 DU in monthly mean VCD) (https://aura.gesdisc.eosdis.nasa.gov/data/Aura_OMI_Level2/OMSO2.003/doc/README.OMSO2.pdf).

Also, PCA retrievals is subject to the systematic bias of 0.7–0.9 DU in relatively high-latitude regions. Located at a

relatively high latitude in northwestern China with a large surrounding area covered by the Gobi desert, the PCA algorithm might yield lower SO₂ VCD value in Ürümqi than other cities shown in Fig. 2.

SO₂ emissions data were further collected to compare with annual OMI SO₂ VCD in selected regions. The results are presented in Fig. 3. As shown, the annual variation in SO₂ VCD agrees reasonably well with SO₂ emission data except for the Ürümqi–Midong region. The OMI-measured SO₂ VCD in the PRD and Sichuan Basin decreased from 2008 to 2012, but SO₂ emissions changed little. Compared with the other five marked regions (Fig. 1), the satellite-measured SO₂ VCD in Ürümqi–Midong decreased in 2010 and increased in 2012. However, SO₂ emissions in Ürümqi–Midong 2012 are factors of 11 and 8 higher than in 2008 and 2010, respectively. It should be noted that air pollutants released in the atmosphere are affected by physical and chemical processes. They may be transported over large distances by atmospheric motions, transformed into other compounds by chemical or photochemical processes, and “washed out” or deposited at the Earth’s surface (Zhao et al., 2017; Brasseur et al., 1998).

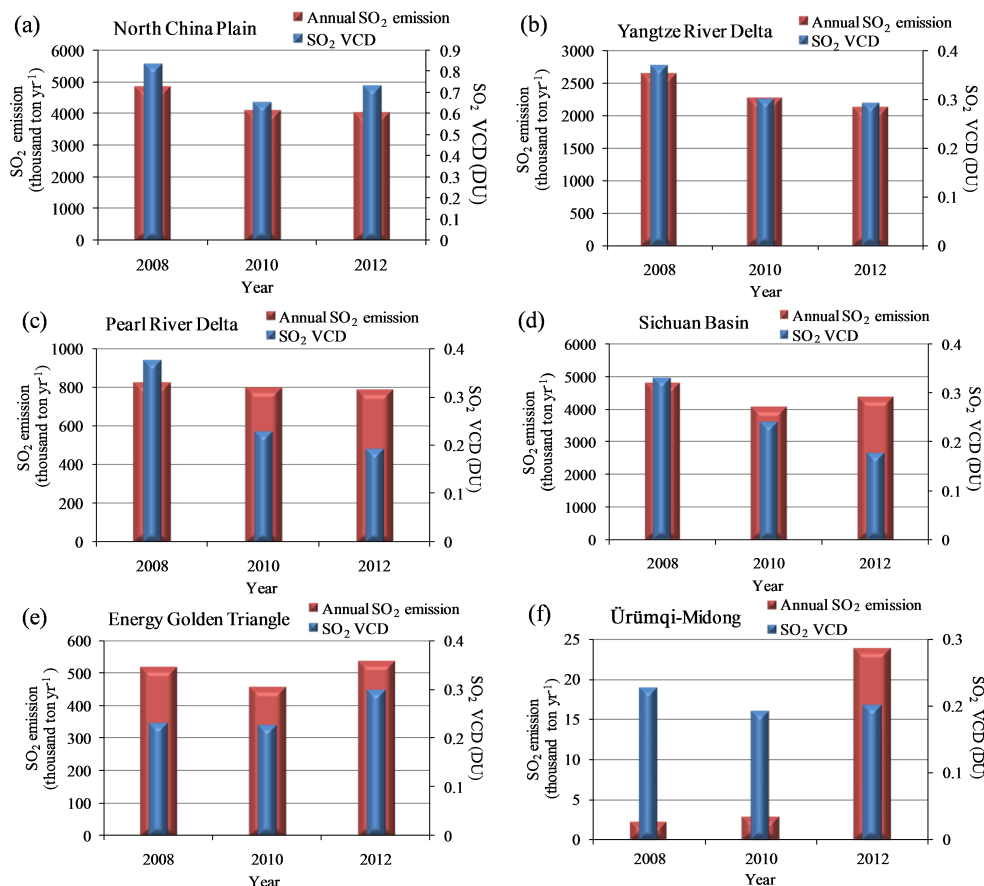


Figure 3. Annually averaged SO₂ VCD (DU), scaled on the right-hand-side y axis, and annual emissions (1000 t yr⁻¹) of SO₂, on the left-hand-side y axis, in the NCP, YRD, PRD, Sichuan Basin, EGT, and Ürümqi–Midong region.

The atmospheric removal and advection processes may also contribute to the inconsistency between monitored and satellite observations. In addition, the MEIC SO₂ emission inventory from the bottom-up approach might be subject to large uncertainties due to data manipulation and the lack of sufficient knowledge in human activities and emissions from different sources (Li et al., 2017; Zhao et al., 2011; Lu et al., 2011; Kurokawa et al., 2013). The uncertainties in the MEIC-estimated SO₂ emissions used in the present study are up to $\pm 12\%$ (Li et al., 2017). As shown in Fig. 3, the OMI-measured SO₂ VCD from 2008 to 2012 in Ürümqi–Midong was about 0.2 DU which was comparable with that in the Energy Golden Triangle (EGT). However, the reported SO₂ emissions in Ürümqi–Midong was only 4 % of the SO₂ emissions in the EGT in 2012 and 0.5 % of that in the EGT from 2008 to 2010. It might be attributed to the fact that some large sources were not included in the MEIC SO₂ emission inventory. From this perspective, the satellite remote sensing provides a very useful tool in monitoring SO₂ emissions from large point sources and in the verification of emission inventories (Fioletov et al., 2015, 2016; McLinden et al., 2016; Wang et al., 2015).

3 Results and discussion

3.1 OMI-measured SO₂ in China

Given higher population density and stronger industrial activities, eastern and southern China is traditionally industrialized and heavily contaminated regions by air pollution and acid rain caused by SO₂ emissions. Figure 4a shows annually averaged OMI SO₂ VCD over China on a $0.25^\circ \times 0.25^\circ$ latitude–longitude resolution averaged from 2005 to 2015. SO₂ VCD was considerably higher in eastern and central China and Sichuan Basin than in northwestern China. The highest SO₂ VCD was found in the NCP, including BTH, Shandong, and Henan. The annually averaged SO₂ VCD between 2005 and 2015 in this region reached 1.36 DU. This result is in line with previous satellite remote-sensing-retrieved SO₂ emissions in eastern China (Krotkov et al., 2016; Lu et al., 2010; Bauduin et al., 2016; Jiang et al., 2012; Yan et al., 2014). However, in contrast to the spatial distribution of decadal mean SO₂ VCD (Fig. 4a), the slopes of the linear regression relationship between annual average OMI-retrieved SO₂ VCD and the time sequence from 2005 to 2015 over

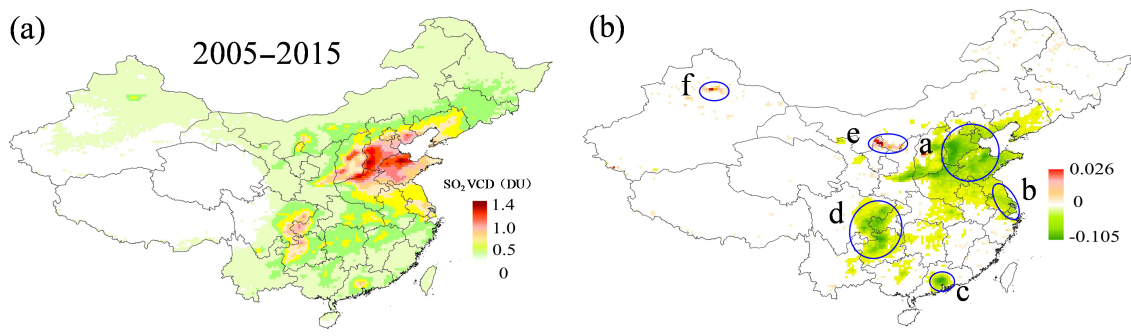


Figure 4. Annual averaging OMI-retrieved vertical column densities of SO₂ (DU) and their trends from 2005 to 2015 on $0.25' \times 0.25'$ latitude–longitude resolution in China. **(a)** Annual mean SO₂ vertical column densities; **(b)** slope (trend) of linear regression relationship between annual averaging OMI-retrieved SO₂ VCD and the time sequence from 2005 to 2015 over China. The positive values indicate an increasing trend of SO₂ VCD from 2005 to 2015, and vice versa. The blue circle highlights the six selected regions including NCP **(a)**, YRD **(b)**, PRD **(c)**, Sichuan Basin **(d)**, Energy Golden Triangle (EGT, **e**), and Ürümqi–Midong region **(f)**.

China show that the negative trends overwhelmed industrialized eastern and southern China, particularly in the NCP, Sichuan Basin, the YRD, and PRD, manifesting a significant decline of SO₂ emissions in these regions. SO₂ VCD in the PRD exhibited the largest decline at a rate of $7\% \text{ yr}^{-1}$, followed by the NCP ($6.7\% \text{ yr}^{-1}$), Sichuan Basin ($6.3\% \text{ yr}^{-1}$), and the YRD ($6\% \text{ yr}^{-1}$). Annual average SO₂ VCD in the PRD, NCP, Sichuan Basin, and YRD decreased by 52, 50, 48, and 46% in 2015 compared to 2005 (Fig. 5), though the annual fluctuation of SO₂ VCD shows rebounds in 2007 and 2011 which are potentially associated with the economic resurgence stimulated by the central government of China (He et al., 2009; Diao et al., 2012). The reduction of SO₂ VCD after 2011 in these regions reflects virtually the response of SO₂ emissions to the regulations in the reduction of SO₂ release, the mandatory application of the flue-gas desulfurization (FGD) on coal-fired power plants and heavy industries, and the slowdown in the growth rate of the Chinese economy (CSC, 2011a; Wang et al., 2015; Chen et al., 2016).

Since in the MK test the signs and fluctuations of UF_k are often used to predict the trend of a time series, this approach is further applied to quantify the trends and step changes in annual SO₂ VCD time series in those highlighted regions (a–f) in Fig. 4b from 2005 to 2015. Results are illustrated in Fig. 6. As shown, the forward and backward sequences UF_k and UB_k intersect at least once from 2005 to 2015. These intersections are all well within the confidence levels between -1.96 and 1.96 at the statistical significance $\alpha = 0.01$. A common feature of the forward sequence UF_k in eastern and southern China provinces is that UF_k has been declining and become negative from 2007 to 2009 onward (Fig. 6a–d), confirming the downturn of SO₂ atmospheric emissions and levels in these industrialized and well-developed regions in China. The step change points of OMI-measured SO₂ VCDs in the NCP, YRD, and Sichuan Basin occurred between 2012 and 2013. These step change points coincide with the im-

plementation of the new Ambient Air Quality Standard in 2012, which set a lower ambient SO₂ concentration limit in the air (MEPC, 2012), and the Air Pollution Prevention and Control Action Plan in 2013 by the State Council of China (CSC, 2013a). This action plan recommends taking immediate actions to control and reduce air pollution in China, including cutting down industrial and mobile emission sources, adjusting industrial and energy structures, and promoting the application of clean energy in the BTH, YRD, PRD, and Sichuan Basin. The step change in SO₂ VCD over the PRD occurred in 2009–2010 and from this period onward the decline of SO₂ VCD speeded up, as shown by the forward sequence UF_k which became negative after 2007 and was below the confidence level of -1.96 after 2009, suggesting significant decreasing VCD from 2009 (Fig. 6c). In April 2002, the Hong Kong Special Administrative Region (HK-SAR) government and the Guangdong provincial government reached a consensus to reduce, on a best endeavor basis, the anthropogenic emissions of SO₂ by 40% in the PRD by 2010, using 1997 as the base year (http://www.epd.gov.hk/epd/english/action_blue_sky/files/exsummary_e.pdf). By the end of 2010, all thermal power units producing more than 0.125 million kW in the PRD were equipped with the FGD. During the 11th 5-year plan (2006–2010), the thermal power units with 1.2 million kilowatts capacity were shut down. SO₂ emissions were reduced by 18% in 2010 compared to that in 2005 (NBSC, 2006, 2011). This likely caused the occurrence of the step change in SO₂ VCD during 2009–2010.

3.2 OMI-measured SO₂ “hot spots” in northwestern China

As also shown in Fig. 4b, in contrast to widespread decline of SO₂ VCD, there are two “hot spots” featured by moderate increasing trends of SO₂ VCD, located in the EGT (Shen et al., 2016; Ma and Xu, 2017) and Ürümqi–Midong region in northwestern China. The annual growth rate of SO₂ VCD

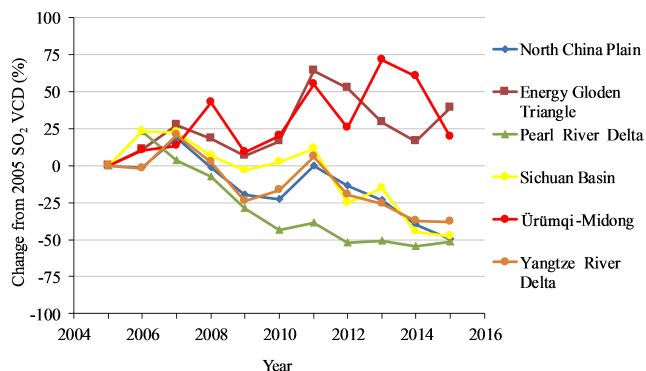


Figure 5. Percentage changes in annual mean OMI SO₂ VCD relative to 2005 in four highlighted regions in eastern and southern China and two large-scale energy industry bases in the EGT and Ürümqi–Midong region in Fig. 4b.

from 2005 to 2015 is 3.4 % yr⁻¹ in the EGT and 1.8 % yr⁻¹ in Ürümqi–Midong (Fig. 4b). SO₂ VCD in these two regions peaked in 2011 and 2013 and was 1.6 and 1.7 times that in 2005 (Fig. 5). The rising SO₂ VCD in the part of the EGT has been reported by Shen et al. (2016). The second hot spot is located in Ürümqi–Midong region, including MEIB, which is about 40 km away from Ürümqi. The EGT and MEIB are both characterized by extensive coal mining, thermal power generation, coal chemical, and coal liquefaction industries. The reserve of coal, oil, and natural gas in the EGT is approximately 1.05×10^{12} t of standard coal equivalent, accounting for 24 % of the national total energy reserve in China (CRGECCR, 2015). It has been estimated that there are deposits of 20.86 billion t of oil, 1.03 billion m³ of natural gas, and 2.19 trillion t of coal in Xinjiang, accounting for 30, 34, and 40 % of the national total (Dou, 2009). Over the past decades, a large number of energy-related industries have been constructed in northwestern China, such as the EGT and MEIB, to enhance China's energy security in the 21st century and speed up the local economy. The rapid development of energy and coal chemical industries in Ningxia Hui Autonomous Region and Xinjiang of northwestern China alone resulted in significant demands to coal mining and coal products. The coal consumption, thermal power generation, and the gross industrial output increased by 2.7, 3.5, and 6.6 times in Ningxia from 2005 to 2015 and by 2.7, 4.2, and 6.6 times in Xinjiang during the same period (NBSC, 2005, 2015). As a result, SO₂ emissions increased markedly in these regions, as shown by the increasing trends of SO₂ VCD in the EGT and Ürümqi–Midong region (Fig. 4b).

The MK forward sequence further confirms the increasing SO₂ VCD in the EGT and Ürümqi–Midong. As seen in Fig. 6e and f, the UF_k values for SO₂ VCD are positive and growing, illustrating clear upward trends of SO₂ VCD over these two large-scale energy industry bases, revealing the response of SO₂ emissions to the energy industry relocation

and development in northwestern China. To guarantee the national energy security and to promote the regional economy, the EGT energy program has been accelerating since 2003 under the national energy development and relocation plan (Zhu and Ruth, 2015; Chen et al., 2016), characterized by the rapid expansion of the NECIB, which is located about 40 km away from Yinchuan, the capital of Ningxia (Shen et al., 2016). By the end of 2010, a large number of coal chemical industries, including the world largest coal liquefaction and thermal power plants, have been built and operated, and the total installed capacity of thermal power generating units has reached 1.47 million kilowatts (Zhao, 2016). Under the same national plan, the MEIB in Xinjiang started construction and operation in the early to mid-2000s and has almost the same type of industry as the EGT, featuring coal-fired power generation, coal chemical industry, and coal liquefaction.

The statistically significant step change points of SO₂ VCD in the EGT and Ürümqi–Midong took place in 2006 and 2009 (Fig. 6e and f), differing from those regions with decreasing trends of SO₂ VCD in eastern and southern China. The first step change point in 2006–2007 corresponds to the increased SO₂ emissions in these two large-scale energy bases until their respective peak emissions in EGT (2007) and Ürümqi–Midong (2008). The second step change point in 2009 coincides with the global financial crisis in 2008, which slowed down the economic growth in 2009 in China considerably, leading to raw material surplus and the remarkable reduction in the demand for coal products.

3.3 OMI SO₂ time series and step change point year in northwestern China

The clearly visible “hot spots” featured by increasing OMI-measured SO₂ VCD in the EGT/NECIB and MEIB raise a question: to what extent could these large-scale energy industrial bases affect the trend and fluctuations of SO₂ emissions in northwestern China? Figure 7 illustrates the fractions (%) of OMI-measured annual SO₂ VCD and SO₂ emissions averaged over the six provinces of northwestern China in the annual national total VCD (Fig. 7a) and emissions (Fig. 7b) from 2005 to 2015. Both the SO₂ VCD and emission fractions in northwestern China in the national total increased over the past decade. By 2015, the mean SO₂ VCD fraction in six northwestern provinces had reached 38 % of the national total. The mean emission fraction was about 20 % in the national total. It should be noted that there were large uncertainties in provincial SO₂ emission data which often underestimated SO₂ emissions from major point sources (Li et al., 2017; Han et al., 2007). In this sense, OMI-retrieved SO₂ VCD fraction provides a more reliable estimate to the contribution of SO₂ emissions in northwestern China to the national total.

The annual percentage changes in SO₂ VCD from 2005 onward are consistent well with the per capita SO₂ emissions

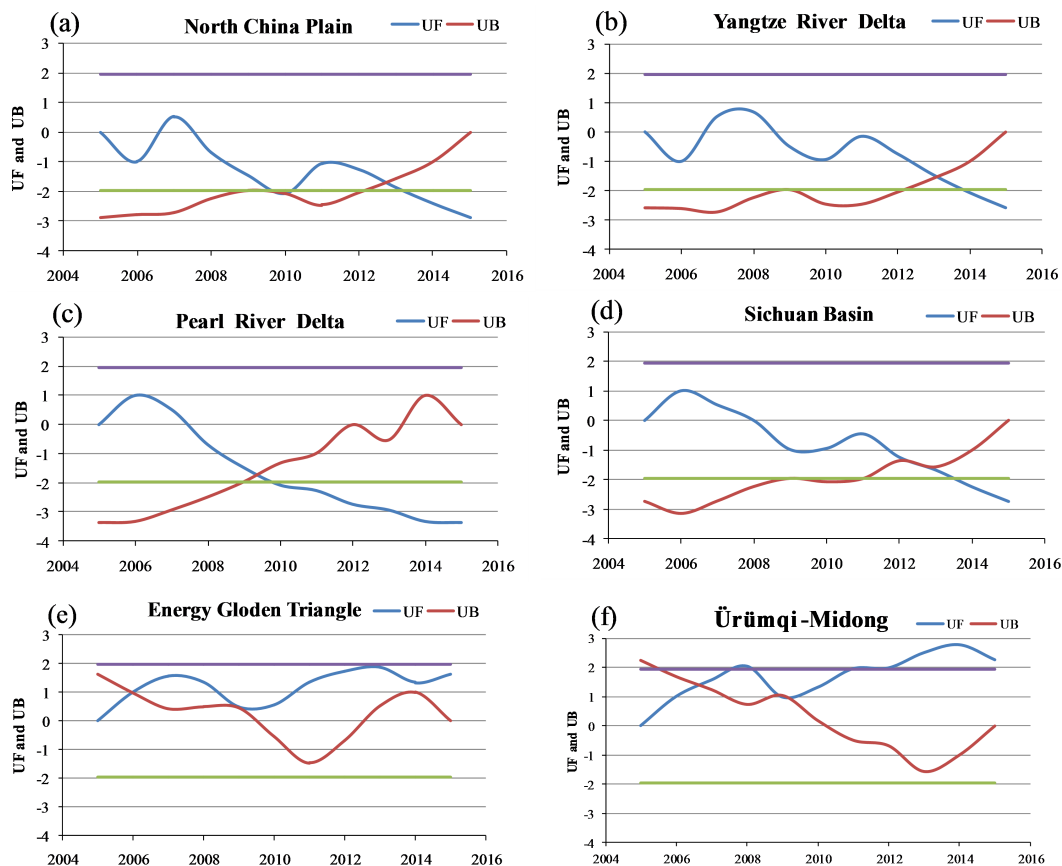


Figure 6. Mann–Kendall (MK) test statistics for annual SO₂ VCD in those highlighted regions (Figs. 1 and 4b) from 2005 to 2015. The blue solid line is the forward sequence UF_k and the red solid line is the backward sequence UB_k defined by Eq. (5). The positive values for UF_k indicate an increasing trend of SO₂ VCD, and vice versa. Two straight solid lines stand for confidence interval between -1.96 (straight green line) and 1.96 (straight purple line) in the MK test. The intersection of UF_k and UB_k sequences within the intervals between two confidence levels indicates a step change point.

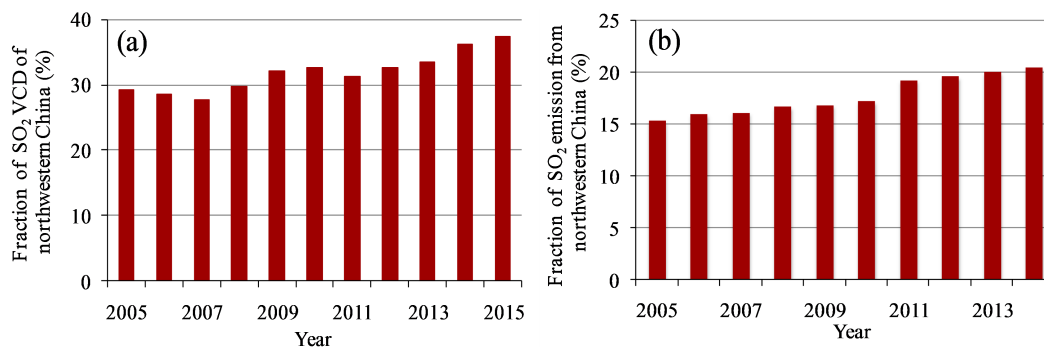


Figure 7. Annual fractions of OMI-retrieved SO₂ VCD and emissions averaged over 6 northwestern provinces in the national total SO₂ VCD from 2005 to 2015 and emissions from 2005 to 2014. **(a)** Fraction of annual mean SO₂ VCD; **(b)** fraction of annual mean emissions. Fractions of SO₂ VCD are calculated as the ratio of the sum of annually averaged SO₂ VCD in northwestern China to the sum of annually averaged SO₂ VCD in the national total from 2005 to 2015 (%).

in China (Fig. 8). As aforementioned, while the annual total SO₂ emissions in the well-developed BTH, YRD, and PRD were higher than in northwestern provinces, the per capita

emissions in all provinces of northwestern China, especially in Ningxia and Xinjiang where the NECIB and MEIB are located, were about factors of 1 to 6 higher than that in the

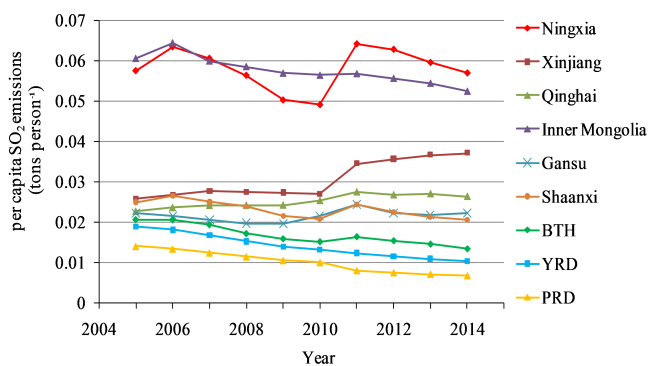


Figure 8. Per capita SO₂ emissions in six provinces of northwestern China and three key eastern regions (t person⁻¹). The value for PRD refers to the per capita SO₂ emissions for Guangdong province.

BTH, YRD, and PRD, as shown in Fig. 8. In contrast to declining annual emissions from the BTH, YRD, and PRD, the per capita SO₂ emissions in almost all western provinces have been growing since 2005.

Since almost all large-scale coal chemical, thermal power generation, and coal liquefaction industries were built in energy-abundant and sparsely populated northwestern China over the past 2 decades, particularly since the early 2000s, those large-scale industrial bases in this part of China likely play an important role in the growing SO₂ emissions in northwestern provinces. We further examine the OMI-retrieved SO₂ VCD to confirm and evaluate the changes in SO₂ emissions in northwestern China which should otherwise respond to these large-scale energy programs under the national plan for energy relocation and expansion. Figure 9 displays the MK test statistics for SO₂ VCD in the six provinces in northwestern China from 2005 to 2015. The forward sequence UF_k suggests decreasing trends in Shaanxi and Gansu provinces and a moderate increase in Qinghai province. In Xinjiang and Ningxia, where the most energy industries were relocated and developed for the last decade (2005–2015), as previously mentioned, UF_k time series estimated using SO₂ VCD data illustrate clear upward trends. Compared with those well-developed regions in eastern and southern China, the UF_k values of SO₂ VCD in these northwestern provinces are almost all positive, except for Shaanxi province where the UF_k turned to negative from 2008 and Gansu province where the UF_k value become negative during 2012–2013.

The step change points identified by the MK test for SO₂ VCD in northwestern China appear strongly associated with the development and use of coal energy. As shown in Fig. 9, the intersection of the forward and backward sequences UF_k and UB_k within the confidence levels of -1.96 (straight green line) to 1.96 (straight purple line) can be identified in 2006 and 2007 in Ningxia and Xinjiang, respectively, corresponding well to the expansion of two largest energy indus-

try bases from 2003 onward in Ningxia (NECIB) and Xinjiang (MEIB). The step change point of SO₂ VCD in 2012 in Gansu province coincides with fuel switching from coal to gas in the capital city (Lanzhou) and many other places of the province initiated from 2012 (CSC, 2013b). The MK-derived step change point in Shaanxi province occurred in 2010, which was a clear signal of marked decline of fossil fuel products in northern Shaanxi (where, as the part of the EGT (Ma and Xu, 2017) of China, the largest energy industry base in the province is located) right after the global financial crisis.

It is interesting to note that the forward sequences UF_k of SO₂ VCD (Fig. 9e and f) in Ningxia and Xinjiang exhibit similar fluctuations as in Ningdong (NECIB) and Ürümqi–Midong (MEIB) (Fig. 9e and f), manifesting the potential associations between the SO₂ emissions in these two large-scale energy industrial bases (major point sources) and provincial emissions in Ningxia and Xinjiang, respectively. This suggests that large-scale energy industrial bases might likely overwhelm or play an important role in the SO₂ emissions in those energy-abundant provinces in northwestern China. Figure 10 illustrates mean SO₂ VCD from 2005 to 2015 in northern Xinjiang (Fig. 10a) and Ningxia (Fig. 10b). The largest concentrations can be seen clearly in the MEIB and the NECIB in these two minority autonomous regions of China. Lower SO₂ concentrations are illustrated in mountainous areas of northern Xinjiang. Based on inverse modeling of SO₂ burdens (a , 10²⁶ molecules) in the source detection model (Sect. 2.4), we estimated SO₂ emissions (E , kt yr⁻¹) in the NECIB and MEIB from 2005 to 2015, defined by $E = a/\tau$, where τ is a decay time of SO₂ (Sect. 2.4). The results are illustrated in Fig. 11. As shown, the SO₂ emissions increased from 2005 and reached the maximum in 2011 in the NECIB and declined thereafter, in line with the annual SO₂ VCD fluctuations in this energy industry base, which is, as already mentioned, attributable to the economic rebound in 2011 in China. Of particular interest are the large fractions of the estimated SO₂ emissions in the NECIB in Ningxia province (Fig. 11a) from 2005 to 2015. These large fractions suggest that this energy industry park alone contributed up to 50 % or more emissions to the provincial total SO₂ emissions. Likewise, the OMI SO₂ VCD-derived SO₂ emissions in the MEIB also made an appreciable contribution (15–20 %) to the provincial total SO₂ emissions in Xinjiang. Covered by a large area of Gobi desert (Junggar Basin), there are only a few SO₂ emission sources in the vast northern Xinjiang region (total area of Xinjiang is 1.66×10^6 km²). This likely leads to the small fractions of SO₂ emissions in the MEIB in the total SO₂ emissions in Xinjiang. Figure 11c and d show SO₂ VCDs (the left y axis) and the ratios (the right y axis) of the mean VCDs in NECIB and MEIB to the provincial mean VCDs in Ningxia and Xinjiang from 2005 to 2015, respectively. It can be seen that the maximum mean SO₂ VCD over the MEIB is about a factor of 4.5 greater than the mean SO₂ VCD over Xinjiang province (Fig. 11d). This ratio

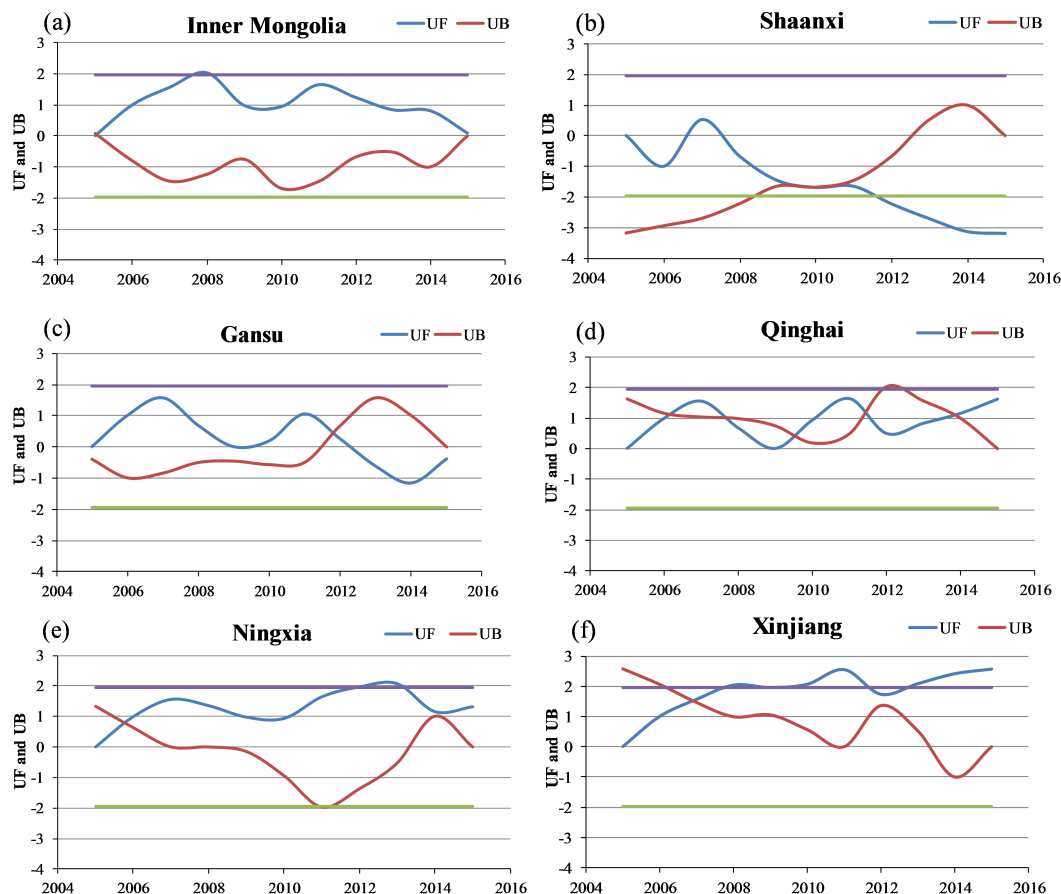


Figure 9. Same as Fig. 6 but for Mann–Kendall (MK) test statistics for annually averaged SO₂ VCD in six provinces in northwestern China from 2005 to 2015.

is larger than the ratio (2.9) of the SO₂ VCD in the NECIB to the SO₂ VCD averaged over Ningxia province (Fig. 11c). Nevertheless, overall our results suggest that, although there were only a small number of SO₂ point sources in these two energy industrial bases, the SO₂ emissions from the NECIB and MEIB made significant contributions to provincial total emissions. Given that the national strategy for China's energy expansion and safety during the 21st century is, to a large extent, to develop large-scale energy industry bases in northwestern China, particularly in Xinjiang and Ningxia (Zhu and Ruth, 2015; Chen et al., 2016) where the energy resources are most abundant in China, we would expect that the rising SO₂ emissions in northwestern China would increasingly be attributed to those large-scale energy industry bases and contribute to the national total SO₂ emissions in China.

Table 1 presents the annual average growth rates of SO₂ VCD, industrial (second) GDP, and major coal-consuming industries in northwestern China and three developed areas (BTH, YRD, PRD) in eastern and southern China. The positive growth rates of SO₂ VCD can be observed in the three provinces and autonomous regions (Qinghai, Ningxia, and Xinjiang) of northwestern China. Although the growth rates

of SO₂ VCD in other two provinces (Gansu and Shaanxi) are negative, the magnitudes of the negative growth rates are smaller than those in the BTH, YRD, and PRD, except for Zhejiang province in the YRD. This regional contrast reflects both their economic and energy development activities and the SO₂ emission control measures implemented by the local and central governments of China. Although China has set a national target of 10 % SO₂ emission reduction (relative to 2005) during 2006–2010 and 8 % (relative to 2010) during 2011–2015 (CSC, 2007, 2011b), under the Grand Western Development Program of China, the regulation for SO₂ emission control was waived in those energy-abundant provinces of northwestern China in order to speed up the large-scale energy industrial bases and local economic development and improve local personal income. Also, although FGDs were widely installed in coal-fired power plants and other industrial sectors since the 1990s, by 2010 as much as 57 % of these systems were installed in eastern and southern China (Zhao et al., 2013). The capacity of small power generators which were shut down in western China was merely about 10 808 MW, only accounting for about 19 % of the capacity of total small power plants which were eliminated

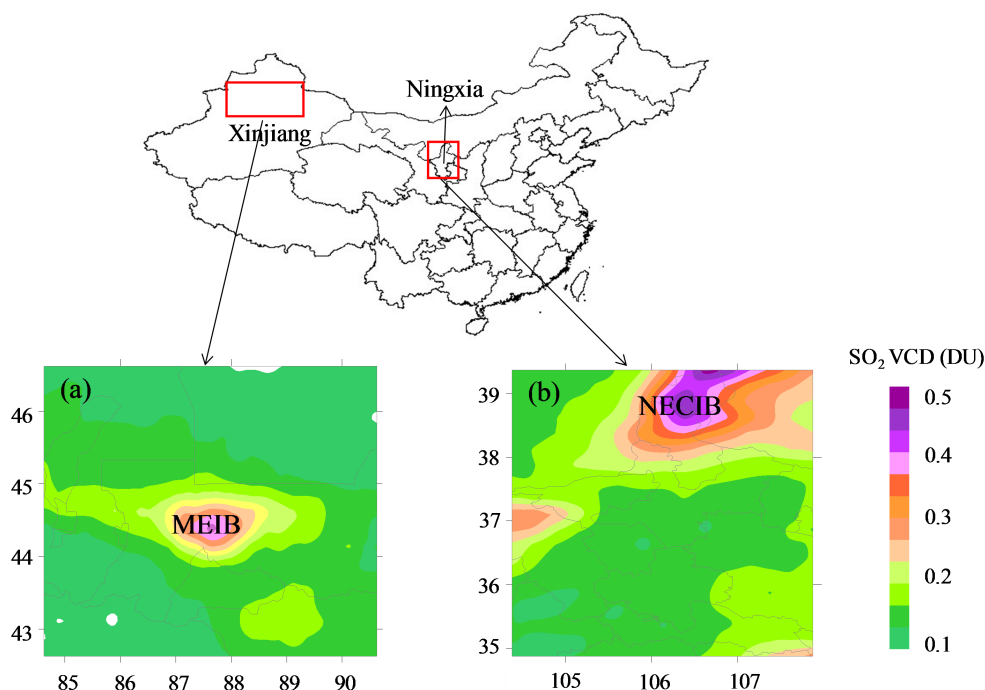


Figure 10. Annually averaging OMI-retrieved vertical column densities of SO₂ (DU) in two major point sources: the MEIB in Xinjiang (a) and the NECIB in Ningxia (b).

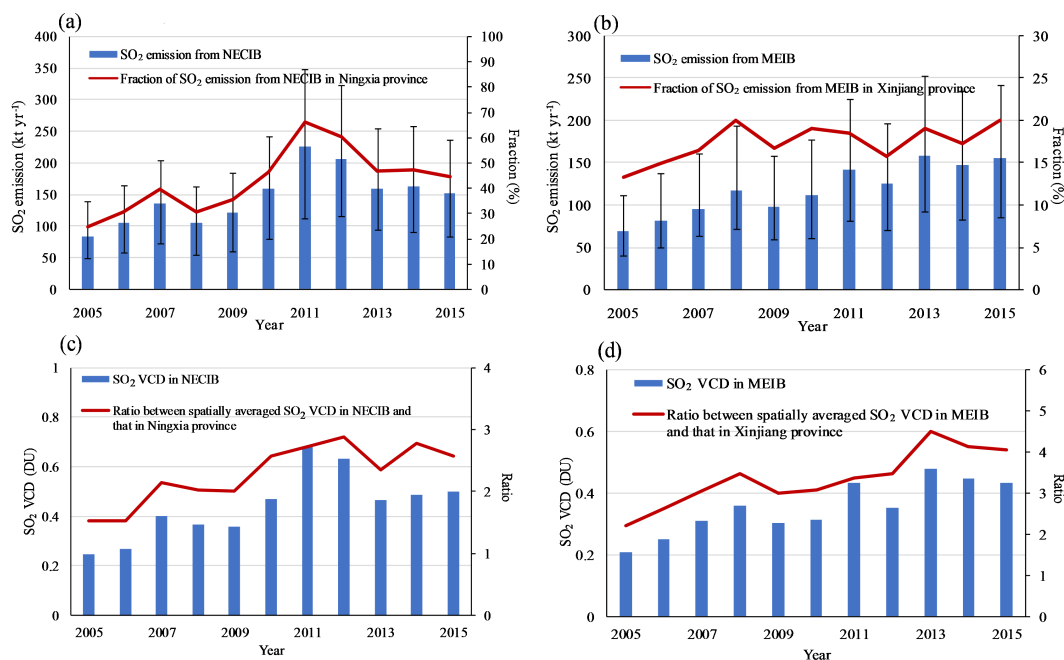


Figure 11. Annually averaged SO₂ emissions (kt yr⁻¹) and SO₂ VCD (DU) in the NECIB and MEIB as well as their fractions in provincial total SO₂ emissions and ratios between SO₂ VCD in these two regions and that in the provinces. (a) SO₂ emissions (blue bar) in the NECIB and its fraction (red solid line) of the total provincial SO₂ emissions in Ningxia. The left y axis is SO₂ emissions, the right y axis denotes the fraction (%) at the upper panel, and the error bars denote the standard deviations of source-detection-algorithm-estimated SO₂ emission point sources; (b) same as Fig. 11a but for the MEIB. (c). SO₂ VCD (blue bar) in the NECIB and the ratio (red solid line) between SO₂ VCD in the NECIB and that in Ningxia. The left y axis stands for SO₂ VCD (DU) and the right y axis denotes the ratio at the lower panel; (d) same as Fig. 11c but for the MEIB.

in China (55 630 MW) during the 11th 5-year plan period (2006–2010) (Cui et al., 2016). As shown in Table 1, the SO₂ emission reduction plans virtually specified the zero percentage of SO₂ emission reductions in Qinghai, Gansu, and Xinjiang and lower reduction percentage in the emission reduction in Ningxia and Inner Mongolia as compared to eastern and southern China during the 11th (2006–2010) and 12th (2011–2015) 5-year plans. As a result, the average growth rate for thermal power generation, steel production, and coal consumption from 2005 to 2015 in northwestern China reached 14.1, 35.7, and 11.9 % yr⁻¹, considerably higher than the averaged growth rates over eastern and southern China (5.9 % yr⁻¹ in the BTH, 0.8 % yr⁻¹ in the YRD, and 2.3 % yr⁻¹ in the PRD).

4 Conclusions

The spatiotemporal variation in SO₂ concentration during 2005–2015 over China was investigated by making use of the PBL SO₂ column concentrations measured by the OMI. The highest SO₂ VCD was found in the NCP, the most heavily SO₂-polluted area in China, including Beijing–Tianjin–Hebei, Shandong, and Henan. Under the national regulation for SO₂ control and emission reduction, the SO₂ VCD in eastern and southern China underwent widespread decline during this period. However, the OMI-measured SO₂ VCD detected two “hot spots” in the EGT (Ningxia–Shaanxi–Inner Mongolia) and Midong (Xinjiang) energy industrial bases, in contrast to the declining SO₂ emissions in eastern and southern China, displaying an increasing trend with the annual growth rate of 3.4 % yr⁻¹ in the EGT and 1.8 % yr⁻¹ in Midong. The trend analysis further revealed enhanced SO₂ emissions in most provinces of northwestern China likely due to the national strategy for energy industry expansion and relocation in energy-abundant northwestern China. As a result, per capita SO₂ emissions in northwestern China have exceeded industrialized and populated eastern and southern China, making increasing contributions to the national total SO₂ emissions. The estimated SO₂ emissions in the Ningdong (Ningxia) and Midong (Xinjiang) energy industrial bases from OMI-measured SO₂ VCD showed that the SO₂ emissions in these two industrial bases made significant contributions to the total provincial emissions. This indicates, on one hand, that the growing SO₂ emissions in northwestern China would increasingly come from those large-scale energy industrial bases under the national energy development and relocation plan. On the other hand, this fact also suggests that it is likely more straightforward to control and reduce SO₂ emissions in northwestern China because the SO₂ control measures could be readily implemented and authorized in those state-owned large-scale energy industrial bases.

Data availability. The OMI SO₂ product (OMSO2 L3 V003) is publicly available from the NASA Goddard Earth Sciences (GES) Data and Information Services Center (DISC) at https://mirador.gsfc.nasa.gov/cgi-bin/mirador/presentNavigation.pl?tree=project&&dataGroup=L3_V003. Other data reported in this article are available upon request. Please contact the corresponding authors, Jianmin Ma (jianminma@lzu.edu.cn) or Tao Huang (huangt@lzu.edu.cn).

The Supplement related to this article is available online at <https://doi.org/10.5194/acp-17-9115-2017-supplement>.

Competing interests. The authors declare that they have no conflict of interest.

Acknowledgements. This work is supported by the National Natural Science Foundation of China (grants 41503089, 41371478, and 41671460), Gansu Province Science and Technology Program for Livelihood of the People (1503FCMA003), the Natural Science Foundation of Gansu Province of China (1506RJZA212), and Fundamental Research Funds for the Central Universities (lzujbky-2016-249 and lzujbky-2016-253). We thank Vitali Fioletov for his suggestions and advice during the preparation of this paper.

Edited by: Leiming Zhang

Reviewed by: two anonymous referees

References

- Assareh, N., Prabamroong, T., Manomaiphiboon, K., Thera-mongkol, P., Leungsakul, S., Mitrjit, N., and Rachiwong, J.: Analysis of observed surface ozone in the dry season over Eastern Thailand during 1997–2012, *Atmos. Res.*, 178, 17–30, <https://doi.org/10.1016/j.atmosres.2016.03.009>, 2016.
- Bauduin, S., Clarisse, L., Hadji-Lazaro, J., Theys, N., Clerbaux, C., and Coheur, P.-F.: Retrieval of near-surface sulfur dioxide (SO₂) concentrations at a global scale using IASI satellite observations, *Atmos. Meas. Tech.*, 9, 721–740, <https://doi.org/10.5194/amt-9-721-2016>, 2016.
- BIEE (British Institute of Energy Economics): BP Statistical Review of World Energy June 2016, available at: <http://www.bp.com/content/dam/bp/pdf/energy-economics/statistical-review-2016/bp-statistical-review-of-world-energy-2016-full-report.pdf> (last access: 21 January 2017), 2016.
- Brasseur, G. P., Hauglustaine, D. A., Walters, S., Rasch, P. J., Müller, J. F., Granier, C., and Tie, X. X.: MOZART, a global chemical transport model for ozone and related chemical tracers: 1. Model description, *J. Geophys. Res.*, 103, 28265–28289, <https://doi.org/10.1029/98JD02397>, 1998.
- Chen, J., Cheng, S., Song, M., and Wang, J.: Interregional differences of coal carbon dioxide emissions in China, *Energ. Policy*, 96, 1–13, <https://doi.org/10.1016/j.enpol.2016.05.015>, 2016.

- CRGECR (The Comprehensive Research Group for Energy Consulting and Research): Strategy on the Development of Energy “Golden Triangle”, *Engineering Science*, 9, 18–28, 2015 (in Chinese).
- CSC (China’s State Council): China National Environmental Protection Plan in the 11th Five-year (2006–2010), available at: http://www.gov.cn/zwggk/2007-11/26/content_815498.htm (last access: 21 January 2017), 2007 (in Chinese).
- CSC (China’s State Council): Circular on accelerating the number of comments on shutting down small thermal power units in China, available at: http://www.gov.cn/zwggk/2007-01/26/content_509911.htm (last access: 21 January 2017), 2011a (in Chinese).
- CSC (China’s State Council): China National Environmental Protection Plan in the 12th Five-year (2011–2015), available at: http://www.gov.cn/zwggk/2011-12/20/content_2024895.htm (last access: 21 January 2017), 2011b (in Chinese).
- CSC (China’s State Council): Air Pollution Prevention and Control Action Plan, available at: http://www.gov.cn/zhengce/content/2013-09/13/content_4561.htm (last access: 21 January 2017), 2013a (in Chinese).
- CSC (China’s State Council): Determination, Measures and Strength-Lanzhou pollution control reproduce the blue sky, available at: http://www.gov.cn/jrzq/2013-02/03/content_2325835.htm (last access: 21 January 2017), 2013b (in Chinese).
- Cui, Y., Lin, J., Song, C., Liu, M., Yan, Y., Xu, Y., and Huang, B.: Rapid growth in nitrogen dioxide pollution over Western China, 2005–2013, *Atmos. Chem. Phys.*, 16, 6207–6221, <https://doi.org/10.5194/acp-16-6207-2016>, 2016.
- Diao, X., Zhang, Y., and Chen, K. Z.: The global recession and China’s stimulus package: A general equilibrium assessment of country level impacts, *China Econ. Rev.*, 23, 1–17, <https://doi.org/10.1016/j.chieco.2011.05.005>, 2012.
- Dou, L.: A research on the impact of industrialization on the environment in Xinjiang with an empirical analysis, MS thesis, Xinjiang University, Urumqi, 2009 (in Chinese).
- Fathian, F., Dehghan, Z., Bazrkar, M. H., and Eslamian, S.: Trends in hydrological and climatic variables affected by four variations of the Mann-Kendall approach in Urmia Lake Basin, Iran, *Hydrolog. Sci. J.*, 61, 892–904, <https://doi.org/10.1080/02626667.2014.932911>, 2016.
- Fioletov, V. E., McLinden, C. A., Krotkov, N., and Li, C.: Lifetimes and emissions of SO₂ from point sources estimated from OMI, *Geophys. Res. Lett.*, 42, 1969–1976, <https://doi.org/10.1002/2015GL063148>, 2015.
- Fioletov, V. E., McLinden, C. A., Krotkov, N., Li, C., Joiner, J., Theys, N., Carn, S., and Moran, M. D.: A global catalogue of large SO₂ sources and emissions derived from the Ozone Monitoring Instrument, *Atmos. Chem. Phys.*, 16, 11497–11519, <https://doi.org/10.5194/acp-16-11497-2016>, 2016.
- Gao, T. and Shi, X.: Spatio-temporal characteristics of extreme precipitation events during 1951–2011 in Shandong, China and possible connection to the large scale atmospheric circulation, *Stoch. Env. Res. Risk. A.*, 30, 1421–1440, <https://doi.org/10.1007/s00477-015-1149-7>, 2016.
- Han, Y., Gao, J., Li, H., and Li, Y.: Ecological suitability analysis on the industry overall arrangement plan of Ningdong energy sources and chemical industry base, *Environ. Sci. Manager*, 32, 142–147, 2007 (in Chinese).
- He, D., Zhang, Z., and Zhang, W.: How large will be the effect of China’s fiscal stimulus package on output and employment, *Pac. Econ. Rev.*, 14, 730–744, <https://doi.org/10.1111/j.1468-0106.2009.00480.x>, 2009.
- Huang, T., Jiang, W., Ling, Z., Zhao, Y., Gao, H., and Ma, J.: Trend of cancer risk of Chinese inhabitants to dioxins due to changes in dietary patterns 1980–2009, *Sci. Rep.*, 6, 21997–22006, <https://doi.org/10.1038/srep21997>, 2016.
- Ialongo, I., Hakkarainen, J., Kivi, R., Anttila, P., Krotkov, N. A., Yang, K., Li, C., Tukiainen, S., Hassinen, S., and Tamminen, J.: Comparison of operational satellite SO₂ products with ground-based observations in northern Finland during the Icelandic Holuhraun fissure eruption, *Atmos. Meas. Tech.*, 8, 2279–2289, <https://doi.org/10.5194/amt-8-2279-2015>, 2015.
- Jiang, J., Zha, Y., Gao, J., and Jiang, J.: Monitoring of SO₂ column concentration change over China from Aura OMI data, *Int. J. Remote Sens.*, 33, 1934–1942, <https://doi.org/10.1080/01431161.2011.603380>, 2012.
- Kanada, M., Dong, L., Fujita, T., Fujita, M., Inoue, T., Hirano, Y., Togawa, T., and Geng, Y.: Regional disparity and cost-effective SO₂ pollution control in China: A case study in 5 mega-cities, *Energ. Policy*, 61, 1322–1331, <https://doi.org/10.1016/j.enpol.2013.05.105>, 2013.
- Kendall, M. G. and Charles, G.: Rank correlation methods, Oxford Univ. Press, New York, USA, 202 pp., 1975.
- Krotkov, N. A., Carn, S. A., Krueger, A. J., Bhartia, P. K., and Yang, K.: Band Residual Difference Algorithm for Retrieval of SO₂ From the Aura Ozone Monitoring Instrument (OMI), *IEEE T. Geosci. Remote*, 44, 1259–1266, <https://doi.org/10.1109/TGRS.2005.861932>, 2006.
- Krotkov, N. A., McClure, B., Dickerson, R. R., Carn, S. A., Li, C., Bhartia, P. K., Yang, K., Krueger, A. J., Li, Z., Levelt, P. F., Chen, H., Wang, P., and Lu, D.: Validation of SO₂ retrievals from the Ozone Monitoring Instrument over NE China, *J. Geophys. Res.*, 113, D16S40, <https://doi.org/10.1029/2007JD008818>, 2008.
- Krotkov, N. A., McLinden, C. A., Li, C., Lamsal, L. N., Celarier, E. A., Marchenko, S. V., Swartz, W. H., Bucsela, E. J., Joiner, J., Duncan, B. N., Boersma, K. F., Veefkind, J. P., Levelt, P. F., Fioletov, V. E., Dickerson, R. R., He, H., Lu, Z., and Streets, D. G.: Aura OMI observations of regional SO₂ and NO₂ pollution changes from 2005 to 2015, *Atmos. Chem. Phys.*, 16, 4605–4629, <https://doi.org/10.5194/acp-16-4605-2016>, 2016.
- Kurokawa, J., Ohara, T., Morikawa, T., Hanayama, S., Janssens-Maenhout, G., Fukui, T., Kawashima, K., and Akimoto, H.: Emissions of air pollutants and greenhouse gases over Asian regions during 2000–2008: Regional Emission inventory in ASia (REAS) version 2, *Atmos. Chem. Phys.*, 13, 11019–11058, <https://doi.org/10.5194/acp-13-11019-2013>, 2013.
- Levelt, P. F., Van der Oord, G. H. J., Dobber, M. R., Malkki, A., Visser, H., De Vries, J., Stammes, P., Lundell, J., Saari, H.: The ozone monitoring instrument. *IEEE T. Geosci. Remote*, 44, 1093–1101, <https://doi.org/10.1109/TGRS.2006.872333>, 2006a.
- Levelt, P. F., Hilsenrath, E., Leppelmeier, G. W., Oord, G. H. J. Van Den, Bhartia, P. K., Tamminen, J., De Haan, J. F., and Veefkind, J. P.: Science Objectives of the Ozone Monitoring Instrument, *IEEE T. Geosci. Remote*, 44, 1199–1208, 2006b.
- Li, C., Zhang, Q., Krotkov, N. A., Streets, D. G., He, K., Tsay, S. C., and Gleason, J. F.: Recent large reduction in sulfur dioxide emissions from Chinese power plants observed by the

- Ozone Monitoring Instrument, *Geophys. Res. Lett.*, 37, L08807, <https://doi.org/10.1029/2010GL042594>, 2010.
- Li, C., Joiner, J., Krotkov, N. A., and Bhartia, P. K.: A fast and sensitive new satellite SO₂ retrieval algorithm based on principal component analysis: Application to the Ozone Monitoring Instrument, *Geophys. Res. Lett.*, 40, 6314–6318, <https://doi.org/10.1002/2013GL058134>, 2013.
- Li, C., Wang, R., Ning, H., and Luo, Q.: Changes in climate extremes and their impact on wheat yield in Tianshan Mountains region, northwest China, *Environ. Earth Sci.*, 75, 1228–1241, <https://doi.org/10.1007/s12665-016-6030-6>, 2016.
- Li, M., Zhang, Q., Kurokawa, J.-I., Woo, J.-H., He, K., Lu, Z., Ohara, T., Song, Y., Streets, D. G., Carmichael, G. R., Cheng, Y., Hong, C., Huo, H., Jiang, X., Kang, S., Liu, F., Su, H., and Zheng, B.: MIX: a mosaic Asian anthropogenic emission inventory under the international collaboration framework of the MICS-Asia and HTAP, *Atmos. Chem. Phys.*, 17, 935–963, <https://doi.org/10.5194/acp-17-935-2017>, 2017.
- Lu, Z., Streets, D. G., Zhang, Q., Wang, S., Carmichael, G. R., Cheng, Y. F., Wei, C., Chin, M., Diehl, T., and Tan, Q.: Sulfur dioxide emissions in China and sulfur trends in East Asia since 2000, *Atmos. Chem. Phys.*, 10, 6311–6331, <https://doi.org/10.5194/acp-10-6311-2010>, 2010.
- Lu, Z., Zhang, Q., and Streets, D. G.: Sulfur dioxide and primary carbonaceous aerosol emissions in China and India, 1996–2010, *Atmos. Chem. Phys.*, 11, 9839–9864, <https://doi.org/10.5194/acp-11-9839-2011>, 2011.
- Ma, J. and Xu, J.: China's energy rush harming ecosystem, *Nature*, 541–30, <https://doi.org/10.1038/541030b>, 2017.
- Mann, H. B.: Nonparametric tests against trend, *Econometrica*, 13, 245–259, <https://doi.org/10.2307/1907187>, 1945.
- McLinden, C. A., Fioletov, V., Boersma, K. F., Kharol, S. K., Krotkov, N., Lamsal, L., Makar, P. A., Martin, R. V., Veefkind, J. P., and Yang, K.: Improved satellite retrievals of NO₂ and SO₂ over the Canadian oil sands and comparisons with surface measurements, *Atmos. Chem. Phys.*, 14, 3637–3656, <https://doi.org/10.5194/acp-14-3637-2014>, 2014.
- McLinden, C. A., Fioletov, V., Krotkov, N. A., Li, C., Boersma, K. F., and Adams, C.: A decade of change in NO₂ and SO₂ over the Canadian oil sands as seen from space, *Environ. Sci. Technol.*, 50, 331–337, <https://doi.org/10.1021/acs.est.5b04985>, 2015.
- McLinden, C. A., Fioletov, V., Shephard, M. W., Krotkov, N., Li, C., Martin, R. V., Moran, M. D., and Joiner, J.: Space-based detection of missing sulfur dioxide sources of global air pollution, *Nat. Geosci.*, 9, 496–500, <https://doi.org/10.1038/ngeo2724>, 2016.
- MEPC (Ministry of Environmental Protection of China): Ambient air quality standards, available at: http://kjs.mep.gov.cn/hjbhbz/bzwb/dqjhbd/dqjzlbz/201203/t20120302_224165.shtml (last access: 21 January 2017), 2012 (in Chinese).
- Moraes, J. M., Pellegrino, G. Q., Ballester, M. V., Martinelli, L. A., Victoria, R. L., and Krusche, A. V.: Trends in hydrological parameters of a southern Brazilian watershed and its relation to human induced changes, *Water Resour. Manag.*, 12, 295–311, <https://doi.org/10.1023/A:1008048212420>, 1998.
- NBSC (National Bureau of Statistics of China): China Energy Statistical Yearbook 2005, China Statistics Press, Beijing, 2005.
- NBSC (National Bureau of Statistics of China): China Energy Statistical Yearbook 2006, China Statistics Press, Beijing, 2006.
- NBSC (National Bureau of Statistics of China): China Energy Statistical Yearbook 2011, China Statistics Press, Beijing, 2011.
- NBSC (National Bureau of Statistics of China): China Energy Statistical Yearbook 2015, China Statistics Press, Beijing, 2015.
- Ohara, T., Akimoto, H., Kurokawa, J., Horii, N., Yamaji, K., Yan, X., and Hayasaka, T.: An Asian emission inventory of anthropogenic emission sources for the period 1980–2020, *Atmos. Chem. Phys.*, 7, 4419–4444, <https://doi.org/10.5194/acp-7-4419-2007>, 2007.
- Sharma, C. S., Panda, S. N., Pradhan, R. P., Singh, A., and Kawamura, A.: Precipitation and temperature changes in eastern India by multiple trend detection methods, *Atmos. Res.*, 180, 211–225, <https://doi.org/10.1016/j.atmosres.2016.04.019>, 2016.
- Shen, Y., Zhang, X., Brook, J. R., Huang, T., Zhao, Y., Gao, H., and Ma, J.: Satellite remote sensing of air quality in the Energy Golden Triangle in Northwest China, *Environ. Sci. Technol. Lett.*, 3, 275–279, <https://doi.org/10.1021/acs.estlett.6b00182>, 2016.
- Sicard, P., Serra, R., and Rossello, P.: Spatiotemporal trends in ground-level ozone concentrations and metrics in France over the time period 1999–2012, *Environ. Res.*, 149, 122–144, <https://doi.org/10.1016/j.envres.2016.05.014>, 2016.
- Smith, S. J., van Aardenne, J., Klimont, Z., Andres, R. J., Volke, A., and Delgado Arias, S.: Anthropogenic sulfur dioxide emissions: 1850–2005, *Atmos. Chem. Phys.*, 11, 1101–1116, <https://doi.org/10.5194/acp-11-1101-2011>, 2011.
- Stevenson, D. S., Johnson, C. E., Collins, W. J., and Derwent, R. G.: The atmospheric sulphur cycle and the role of volcanic SO₂, *Geol. Soc. Lond. Spec. Publ.*, 213, 295–305, <https://doi.org/10.1144/GSL.SP.2003.213.01.18>, 2003.
- Su, S., Li, B., Cui, S., and Tao, S.: Sulfur Dioxide Emissions from Combustion in China: From 1990 to 2007, *Environ. Sci. Technol.*, 45, 8403–8410, <https://doi.org/10.1021/es201656f>, 2011.
- Waked, A., Sauvage, S., Borbon, A., Gauduin, J., Pallares, C., Vagnot, M. P., Thierry, L., and Locoge, N.: Multi-year levels and trends of non-methane hydrocarbon concentrations observed in ambient air in France, *Atmos. Environ.*, 141, 263–275, <https://doi.org/10.1016/j.atmosenv.2016.06.059>, 2016.
- Wang, S.: Satellite remote sensing of the sulfur dioxide and nitrogen dioxide emissions from coal-fired power plants, PhD thesis, Tsinghua University, Beijing, 2014.
- Wang, S., Zhang, Q., Martin, R. V., Philip, S., Liu, F., Li, M., Jiang, X., and He, K.: Satellite measurements oversee China's sulfur dioxide emission reductions from coal-fired power plants, *Environ. Res. Lett.*, 10, 114015, <https://doi.org/10.1088/1748-9326/10/11/114015>, 2015.
- Wang, Z., Shao, M., Chen, L., Tao, M., Zhong, L., Chen, D., Fan, M., Wang, Y., and Wang, X.: Space view of the decadal variation for typical air pollutants in the Pearl River Delta (PRD) region in China, *Front. Env. Sci. Eng.*, 10, 9–22, <https://doi.org/10.1007/s11783-016-0853-y>, 2016.
- Whelpdale, D. M., Dorling, S. R., Hicks, B. B., and Summers, P. W.: Atmospheric process in: Global Acid Deposition Assessment, edited by: Whelpdale, D. M. and Kaiser, M. S., World Meteorological Organization Global Atmosphere Watch, Report Number 106, Geneva, 7–32, 1996.
- Yan, H., Chen, L., Su, L., Tao, J., and Yu, C.: SO₂ columns over China: Temporal and spatial variations using OMI and GOME-2 observations, 35th International Symposium on Remote Sens-

- ing of Environment, 17, 012027, <https://doi.org/10.1088/1755-1315/17/1/012027>, 2014.
- Yue, S. and Pilon, P.: A comparison of the power of the t-test, Mann-Kendall and bootstrap tests for trend detection, *Hydrolog. Sci. J.*, 49, 21–37, <https://doi.org/10.1623/hysj.49.1.21.53996>, 2004.
- Yue, S. and Wang, C.: The Mann-Kendall test modified by effective sample size to detect trend in serially correlated hydrological series, *Water Resour. Manag.*, 18, 201–218, <https://doi.org/10.1023/B:WARM.0000043140.61082.60>, 2004.
- Zhang, X., Huang, T., Zhang, L., Gao, H., Shen, Y., and Ma, J.: Trends of deposition fluxes and loadings of sulfur dioxide and nitrogen oxides in the artificial Three Northern Regions Shelter Forest across northern China, *Environ. Pollut.*, 207, 238–247, <https://doi.org/10.1016/j.envpol.2015.09.022>, 2015.
- Zhang, X., Huang, T., Zhang, L., Shen, Y., Zhao, Y., Gao, H., Mao, X., Jia, C., and Ma, J.: Three-North Shelter Forest Program contribution to long-term increasing trends of biogenic isoprene emissions in northern China, *Atmos. Chem. Phys.*, 16, 6949–6960, <https://doi.org/10.5194/acp-16-6949-2016>, 2016.
- Zhang, Y., Guan, D., Jin, C., Wang, A., Wu, J., and Yuan, F.: Analysis of impacts of climate variability and human activity on stream flow for a river basin in northeast China, *J. Hydrol.*, 410, 239–247, <https://doi.org/10.1016/j.jhydrol.2011.09.023>, 2011.
- Zhao, B., Wang, S. X., Liu, H., Xu, J. Y., Fu, K., Klimont, Z., Hao, J. M., He, K. B., Cofala, J., and Amann, M.: NO_x emissions in China: historical trends and future perspectives, *Atmos. Chem. Phys.*, 13, 9869–9897, <https://doi.org/10.5194/acp-13-9869-2013>, 2013.
- Zhao, H., Li, X., Zhang, Q., Jiang, X., Lin, J., Peters, G. G., Li, M., Geng, G., Zheng, B., Huo, H., Zhang, L., Davis, S. J., and He, K.: Effects of atmospheric transport and trade on air pollution mortality in China, *Atmos. Chem. Phys. Discuss.*, <https://doi.org/10.5194/acp-2017-263>, in review, 2017.
- Zhao, L.: Strategic thinking on construction of Ningdong Energy Chemical Base and development of Ningxia Coal Industry Group, *Northwest Coal*, 4, 11–13, 2016 (in Chinese).
- Zhao, Y., Nielsen, C. P., Lei, Y., McElroy, M. B., and Hao, J.: Quantifying the uncertainties of a bottom-up emission inventory of anthropogenic atmospheric pollutants in China, *Atmos. Chem. Phys.*, 11, 2295–2308, <https://doi.org/10.5194/acp-11-2295-2011>, 2011.
- Zhao, Y., Huang, T., Wang, L., Gao, H., and Ma, J.: Step changes in persistent organic pollutants over the Arctic and their implications, *Atmos. Chem. Phys.*, 15, 3479–3495, <https://doi.org/10.5194/acp-15-3479-2015>, 2015.
- Zhu, J. and Ruth, M.: Relocation or reallocation: Impacts of differentiated energy saving regulation on manufacturing industries in China, *Ecol. Econ.*, 110, 119–133, <https://doi.org/10.1016/j.ecolecon.2014.12.020>, 2015.